

Direct torque control of induction machine fed by 5-level flying capacitor inverter with active balancing strategy for electric vehicle application

Abstract. In electric vehicle (EV), control strategies play a key role in vehicle dynamic behavior and stability. The traction chain considered in this article consists of a multilevel inverter, an induction machine (IM) and open differential. The proposed control strategy is based on DTC drive. Moreover, In this paper we present, on the one hand, the contribution provided by 5-level flying capacitor inverter with active balancing in DTC control and, on the other hand, the application of the global structure proposed with 7 degrees of freedom (7-DOF) EV model. Computer simulations were performed using the Matlab/Simulink environment to evaluate the performance of the proposed control.

Streszczenie. W pojeździe elektrycznym (EV) strategie sterowania odgrywają kluczową rolę w dynamicznym zachowaniu i stabilności pojazdu. Łańcuch trakcyjny rozważany w tym artykule składa się z falownika wielopoziomowego, maszyny indukcyjnej (IM) oraz otwartego mechanizmu różnicowego. Zaproponowana strategia sterowania oparta jest na napędzie DTC. Ponadto w artykule przedstawiono z jednej strony wkład wniesiony przez 5-poziomowy falownik latającego kondensatora z aktywnym równoważeniem w sterowaniu DTC, a z drugiej strony zastosowanie globalnej struktury zaproponowanej z 7 stopniami swobody (7-DOF) Model EV. Przeprowadzono symulacje komputerowe z wykorzystaniem środowiska Matlab/Simulink w celu oceny działania proponowanego sterowania. (Bezpośrednie sterowanie momentem obrotowym maszyny indukcyjnej zasilanej przez 5-poziomowy latający falownik kondensatorowy z aktywną strategią równoważenia do zastosowania w pojazdach elektrycznych)

Keywords: DTC, active balancing, flying capacitor inverter, electric vehicle, RWD, 7-DOF

Słowa kluczowe: DTC, aktywne równoważenie, falownik kondensatorowy, Pojazd elektryczny, RWD, 7-DOF

Introduction

The electric vehicles (EVs) offers one of the best solution to the atmosphere pollution problem. Much research has been done to develop EVs in terms of electric propulsion system control.

In this work, it is based on the Direct Torque Control (DTC), with this strategy the electromagnetic torque and the stator flux are controlled by the direct determination of control sequences applied to the switches of voltage-source inverter (VSI). The main advantages of this drive are: Easy to design and implement, lower sensibility to parametric variations (stator resistance the only factor affecting the DTC) [1], and very quick responses of torque and flux. However, the DTC presents also some drawbacks such as: High torque and stator flux ripples [1], and current distortion. To circumvent some of those disadvantages and improve the DTC control, several authors have proposed the use of multilevel inverter for DTC drive [2], [3].

This paper describes control scheme for DTC of induction machine with five level flying capacitor inverter, the DTC concept does not change, as in the case of 2-level inverter, 2 hysteresis comparators and look-up table, but levels of hysteresis comparators are increased to compensate the large number of available voltage vectors in 5-level inverter, the maximum voltage stress and switching frequency across the switches decrease considerably with increasing level of inverter.

The flexibility provided by 5-level flying capacitor inverter is unfortunately accompanied by the problem of capacitor voltage variation that it needs to be corrected. Various solutions were suggested to balance capacitor voltages of multilevel flying capacitor inverter [4, 5, 6] through the control of PWM (Pulse Width Modulation). However, in our case, we look for a direct control of switches for balancing, which can adapt to direct aspect of DTC strategy, therefore, an elegant way to exploit multilevel inverter for dtc control is through an active balancing of capacitor voltages basing it only on configuration selction by each leg of inverter [7].

The control proposed is used for electric vehicle control, for this reason, on present a 7 degrees of freedom (7-DOF) vehicle model with rear wheel drive (RWD) architecture controlled by induction machine via an open differential.

The rest of the paper is structured as follows: Section II presents the model of induction machine. The 5-level flying capacitor inverter is introduced in section III. Section IV presents the active balancing of capacitor voltages of inverter. Section V describes direct torque control using 5-level inverter. Section VI presents electric vehicle design and modeling. The combined slip tire model and driver model are introduced in section VII and section VIII. Section IX shows the simulation results. Analysis and discussion of these results are given in section X and section XI. Finally, the section XII concludes the work.

Mathematical model of induction machine

Model of the induction motor is presented in the stationary (α, β) reference frame in the state equation form as follows:

$$(1) \quad \dot{X} = AX + BU$$

Such as:

$$(2) \quad X = [I_{s\alpha} \ I_{s\beta} \ \phi_{s\alpha} \ \phi_{s\beta}]^T, \quad U = [V_{s\alpha} \ V_{s\beta}]^T$$

$$(3) \quad A = \begin{bmatrix} -\frac{1}{\sigma} + \left(\frac{1}{T_r} + \frac{1}{T_s}\right) & -\omega_r & \frac{1}{\sigma L_s T_r} & \frac{\omega_r}{\sigma L_s} \\ \omega_r & -\frac{1}{\sigma} + \left(\frac{1}{T_r} + \frac{1}{T_s}\right) & -\frac{\omega_r}{\sigma L_s} & \frac{1}{\sigma L_s T_r} \\ R_s & 0 & 0 & 0 \\ 0 & R_s & 0 & 0 \end{bmatrix}$$

$$(4) \quad B = \begin{bmatrix} \frac{1}{\sigma L_s} & 0 \\ 0 & \frac{1}{\sigma L_s} \\ 1 & 0 \\ 0 & 1 \end{bmatrix}, \quad \sigma = 1 - \frac{M^2}{L_s L_r}$$

$$(5) \quad T_s = \frac{L_s}{R_s}, \quad T_r = \frac{L_r}{R_r}$$

The expression of electromagnetic torque can be given by:

$$(6) \quad T_{em} = \frac{3}{2} P (\phi_{s\alpha} I_{s\beta} - \phi_{s\beta} I_{s\alpha})$$

The mechanical equation of the IM can be written as follows:

$$(7) \quad J_m \dot{\Omega}_r = T_{em} - T_m - f_r \Omega_r$$

Where: $V_{s\alpha}$, $V_{s\beta}$, $I_{s\alpha}$, $I_{s\beta}$, $\phi_{s\alpha}$, $\phi_{s\beta}$ – stator voltage, stator current, stator flux in (α, β) reference frame respectively. T_s, T_r – the stator and rotor time constant respectively. σ – the dispersion coefficient of the machine. T_m – load torque.

5-Level flying capacitor inverter

The principle of this topology is to split the DC bus voltage into several elementary voltage sources.

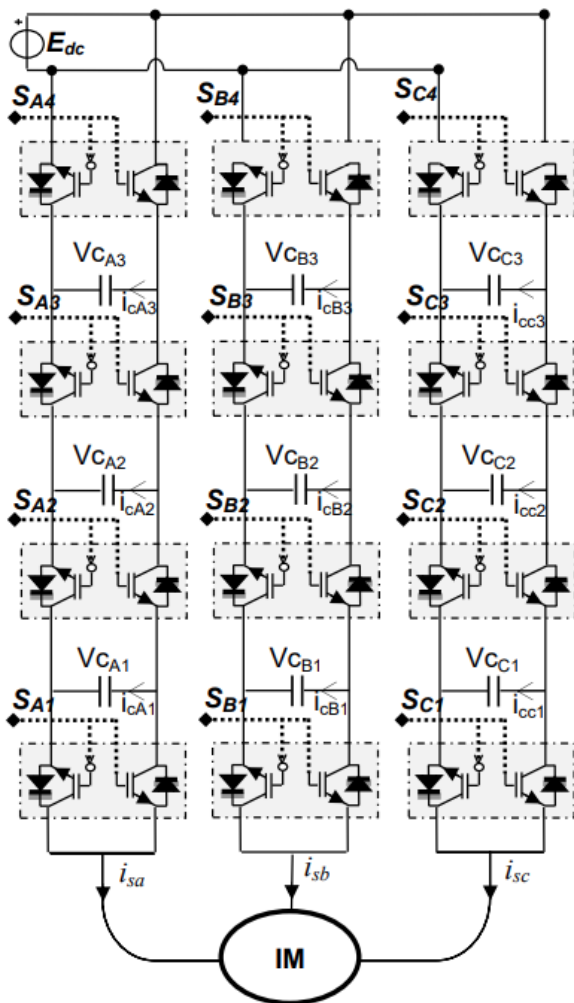


Fig.1. Three-phase 5-Level flying capacitor inverter topology

Fig. 1 shows a three phase induction machine supplied by 5-level flying capacitor inverter, each leg of this type of inverter is composed by 4 switching cells and 3 flying capacitors, to void short-circuit condition, the two switches of each cell must operate in complementary mode. For leg-A, the output leg to ground voltage can be written as:

$$(8) \quad V_A = \sum_{i=1}^4 S_{Ai} V_{cell i}$$

The voltage of cell_i is given by:

$$(9) \quad V_{cell i} = V_{ca i+1} - V_{ca i}$$

Where: $V_{ca0}=0$ and $V_{ca4}=E_{dc}$.

The capacitor current is given by:

$$(10) \quad I_{CA i} = (S_{A i+1} - S_{A i}) I_{SA}$$

The active balancing of capacitor voltages

In order to show the influence of different possible configurations per leg on capacitor voltages variation, we present the table.1, we note that the intermediate voltages ($E_{dc}/4, 2E_{dc}/4, 3E_{dc}/4$) can be generated by several configurations which increase and decrease the flying voltages ($V_{ca1}, V_{ca2}, V_{ca3}$). The permutation between these configurations can keep capacitor voltages at their reference values using hysteresis comparator (see Fig. 2).

Hysteresis bands H_{vca1}, H_{vca2} and H_{vca3} will be fixed to 1 Volts. This technique has already proposed by [7], and tested on 4-level flying capacitor inverter, the same strategy is applied in this work for 5-level inverter. Fig. 2 shows the basic structure of this type of balancing.

Table 1. Variation of capacitor voltages- leg A

configurations [S _{A1} S _{A2} S _{A3} S _{A4}]	Leg to ground voltage V _A	I _{sa} >0			I _{sa} <0		
		V _{CA1}	V _{CA2}	V _{CA3}	V _{CA1}	V _{CA2}	V _{CA3}
0: [0 0 0 0]	0	≈	≈	≈	≈	≈	≈
1: [0 0 0 1]	E _c /4	↓	≈	≈	↑	≈	≈
2: [0 0 1 0]	E _c /4	↑	↓	≈	↓	↑	≈
3: [0 0 1 1]	2*E _c /4	≈	↑	≈	≈	↑	≈
4: [0 1 0 0]	E _c /4	≈	↓	≈	≈	↓	≈
5: [0 1 0 1]	2*E _c /4	↓	↑	≈	↑	↓	≈
6: [0 1 1 0]	2*E _c /4	↑	≈	≈	↓	≈	≈
7: [0 1 1 1]	3*E _c /4	≈	≈	≈	≈	≈	≈
8: [1 0 0 0]	E _c /4	≈	≈	≈	≈	≈	≈
9: [1 0 0 1]	2*E _c /4	↓	≈	≈	↑	≈	≈
10: [1 0 1 0]	2*E _c /4	≈	↓	≈	≈	↑	≈
11: [1 0 1 1]	3*E _c /4	≈	≈	≈	≈	≈	≈
12: [1 1 0 0]	2*E _c /4	≈	↑	≈	≈	≈	≈
13: [1 1 0 1]	3*E _c /4	↓	↑	≈	≈	≈	≈
14: [1 1 1 0]	3*E _c /4	↑	≈	≈	≈	≈	≈
15: [1 1 1 1]	E _c	≈	≈	≈	≈	≈	≈

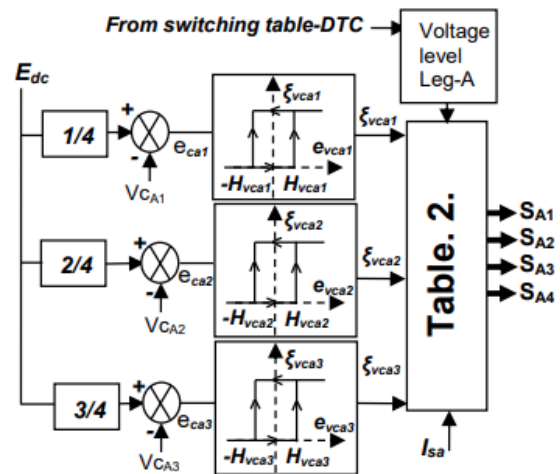


Fig.2. Active balancing by leg for 5-level flying capacitor inverter

Table. 2. Configuration selection for active balancing of 5-level flying capacitor inverter

voltage level [ξ_{vca3} ξ_{vca2} ξ_{vca1}]	0	Ec/4	2*Ec/4	3*Ec/4	Ec
	0: [0 0 0]	0	1	3	7
1: [0 0 1]	0	2			15
2: [0 1 0]	0		5		15
3: [0 1 1]	0	4			15
4: [1 0 0]	0			11	15
5: [1 0 1]	0		10		15
6: [1 1 0]	0			13	15
7: [1 1 1]	0	8	12	14	15

The errors e_{ca1} , e_{ca2} and e_{ca3} between reference values $E_{dc}/4$, $2*E_{dc}/4$, $3*E_{dc}/4$ and the capacitor voltages V_{ca1} , V_{ca2} and V_{ca3} respectively, will be introduced in 2-level Hysteresis comparators with boolean variable output (0,1). where: 0 – not increasing the capacitor voltage, 1 – not decreasing the capacitor voltage.

Note that, It was necessary to use voltage sensors in order to determine V_{ca1} , V_{ca2} and V_{ca3} .

The empty boxes of Table. 2 indicate that there is no configuration to satisfy at the same time the three conditions (ξ_{vca1} ξ_{vca2} ξ_{vca3}), thus, we determine the optimal choice according to capacitor voltage errors (e_{ca1} , e_{ca2} , e_{ca3}), therefore, we define:

$$(11) \quad E_{ca1} = e_{ca1}/(E_{dc}/4)$$

$$(12) \quad E_{ca2} = e_{ca2}/(2 * E_{dc}/4)$$

$$(13) \quad E_{ca3} = e_{ca3}/(3 * E_{dc}/4)$$

The empty-cells will be completed as follows:

$$(14) \quad cell(2; Ec/4) = \begin{cases} 1, & \text{if } E_{ca1} \geq E_{ca2} \text{ and } E_{ca1} \geq E_{ca3} \\ 4, & \text{else} \end{cases}$$

$$(15) \quad cell(4; Ec/4) = \begin{cases} 1, & \text{if } E_{ca1} \geq E_{ca3} \\ 8, & \text{else} \end{cases}$$

$$(16) \quad cell(5; Ec/4) = \begin{cases} 8, & \text{if } E_{ca1} < E_{ca3} \text{ and } E_{ca3} \geq E_{ca2} \\ 2, & \text{else} \end{cases}$$

$$(17) \quad cell(6; Ec/4) = \begin{cases} 8, & \text{if } E_{ca1} < E_{ca3} \\ 1, & \text{else} \end{cases}$$

$$(18) \quad cell(1; 2 * Ec/4) = \begin{cases} 3, & \text{if } E_{ca1} < E_{ca2} \text{ and } E_{ca3} < E_{ca2} \\ 6, & \text{else} \end{cases}$$

$$(19) \quad cell(3; 2 * Ec/4) = \begin{cases} 12, & \text{if } E_{ca1} < E_{ca2} \text{ and } E_{ca3} < E_{ca2} \\ 6, & \text{else} \end{cases}$$

$$(20) \quad cell(4; 2 * Ec/4) = \begin{cases} 3, & \text{if } E_{ca1} < E_{ca2} \text{ and } E_{ca3} < E_{ca2} \\ 9, & \text{else} \end{cases}$$

$$(21) \quad cell(6; 2 * Ec/4) = \begin{cases} 12, & \text{if } E_{ca1} < E_{ca2} \text{ and } E_{ca3} < E_{ca2} \\ 9, & \text{else} \end{cases}$$

$$(22) \quad cell(1; 3 * Ec/4) = \begin{cases} 14, & \text{if } E_{ca1} < E_{ca3} \\ 7, & \text{else} \end{cases}$$

$$(23) \quad cell(2; 3 * Ec/4) = \begin{cases} 7, & \text{if } E_{ca1} < E_{ca3} \text{ and } E_{ca3} \geq E_{ca2} \\ 13, & \text{else} \end{cases}$$

$$(24) \quad cell(3; 3 * Ec/4) = \begin{cases} 7, & \text{if } E_{ca1} < E_{ca3} \\ 14, & \text{else} \end{cases}$$

$$(25) \quad cell(5; 3 * Ec/4) = \begin{cases} 14, & \text{if } E_{ca1} \geq E_{ca2} \text{ and } E_{ca1} \geq E_{ca3} \\ 11, & \text{else} \end{cases}$$

Note that, the strategy will be the same for the other legs (leg-b and leg-c), thus offering the advantage of the independence active balancing between three legs.

Direct torque control with multilevel inverter

Main idea of this technique is the direct determination of control sequences (voltage vectors) applied to the switches of voltage-source inverter (VSI) in very short intervals (sampling period T_e), which forces the torque and the stator flux to track reference values.

In the stationary (α, β) reference, the stator voltage can be given by:

$$(26) \quad V_s = R_s I_s + d\phi_s/dt$$

We can assume that for a small time interval, the term ($R_s I_s$) very low and can be neglected, the equation (26) becomes:

$$(27) \quad V_s \approx d\phi_s/dt$$

Equation (27) shows that the stator flux vector Φ_s can be controled directly by stator voltage vector.

The electromagnetic torque of induction machine given in (5) can be rewritten as:

$$(28) \quad T_{em} = P \frac{M}{\sigma L_s L_r} \|\phi_s\| \|\phi_r\| \sin \gamma$$

Where: γ – the angle between stator and rotor flux space vectors.

stator flux magnitude can be obtained as:

$$(29) \quad \|\phi_s\| = \sqrt{\phi_{s\alpha}^2 + \phi_{s\beta}^2}$$

stator flux angle θ_s can be given as:

$$(30) \quad \theta_s = \tan^{-1} \frac{\phi_{s\beta}}{\phi_{s\alpha}}$$

Thus, from equations 1 et 2, the torque control is feasible by the choice of V_s , if three conditions are met, first, keeping the stator flux magnitude constant at the reference value, second, changing the angle γ in the desired direction, three, keeping rotor flux position constant during γ variation, for the last condition just using a sampling period $T_e \ll \sigma T_r$ is sufficient because rotor flux vector changes slower than the stator flux. The other two conditions are achieved by the use of Hysteresis comparators and switching table.

A five level flying capacitor inverter can assume a total of 61 voltage vectors (see Fig. 3) with 125 switching states, in general the voltage vectors can be classified into nine groups according to their magnitudes: (V0); (V1 to V6); (V8, V10, V12, V14, V16, V18); (V7, V9, V11, V13, V15, V17); (V20, V21, V23, V24, V26, V27, V29, V30, V32, V33, V35, V36); (V19, V22, V25, V28, V31, V34); (V39, V43, V47, V51, V55, V59); (V38, V40, V42, V44, V46, V48, V50, V52, V54, V56, V58, V60); (V37, V41, V45, V49, V53, V57).

Voltage vectors availability in 5-level flying capacitor inverter (see Fig. 3) provide the advantage to increase the level of hysteresis comparators [8, 9]. In this work, we use 9-level Hysteresis comparator for electromagnetic torque and 3-level for stator flux. Note that, stator flux space has been split into 12 sectors of 30° degrees and for switching table, we prefer using the look-up table presented in [10].

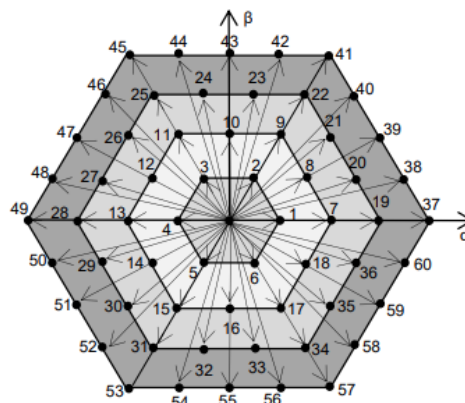


Fig.3. Voltage space vectors for 5-level flying capacitor inverter

The electric vehicle application require a wide speed range of operation which exceeds the rated speed of induction machine. For a fixed DC voltage (E_{dc}), the torque capability decrease after rated speed (Ω_b) and the stator

flux reference in DTC control must be decreased (field weakening region) (see Fig. 4).

Several authors have proposed the improvement of field weakening strategy [11, 12, 13]. In this article, we are satisfied to use the classical field weakening method as given by the following expression [14]:

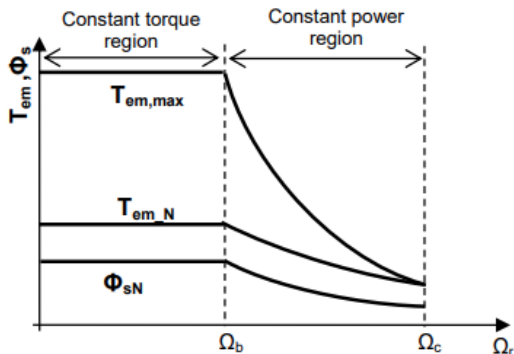


Fig.4. Torque limiting in the field-weakening region

$$(31) \quad \Phi_{s_ref} = \begin{cases} \Phi_{s_ref_nominal} & \text{if } |\Omega_r| \leq |\Omega_b| \\ \Phi_{s_ref_nominal} \frac{\Omega_b}{\Omega_r} & \text{if } |\Omega_b| < |\Omega_r| \leq |\Omega_c| \end{cases}$$

It is assumed that the critical speed was obtained as [15]:

$$(32) \quad \Omega_c = 2.5\Omega_b$$

As consequence of the above, the torque reference T_{em_ref} will be limited as:

$$(33) \quad T_{em_ref_sat} = \min\left(T_{em_ref}; T_{rated} \frac{\Omega_b}{\Omega_r}\right)$$

Fig. 5 shows Proposed structure of DTC scheme for induction machine fed by 5 level flying capacitor inverter with active balancing.

Electric Vehicle design and modeling

In this work, the electric-vehicle drivetrain architecture used is Rear Wheel Drive (RWD) with a single induction motor driving two rear wheels through an open differential (see Fig. 7). For detailed study of the electric vehicle behavior, a Seven Degrees-Of-Freedom (7-dof) vehicle model is developed [16, 17], including longitudinal motion, lateral motion, yaw motion and the spin of four wheels as shown in Fig. 6.

The equations of the vehicle motion are expressed as:

$$(34) \quad m_v a_x = m_v (\dot{v}_x - \psi \dot{v}_y) = (F_{xfl} + F_{xfr}) \cos \delta - (F_{yfl} + F_{yfr}) \sin \delta + F_{xrl} + F_{xrr} - F_a - F_g - F_r$$

$$(35) \quad m_v a_y = m_v (\dot{v}_y + \psi \dot{v}_x) = (F_{yfl} + F_{yfr}) \cos \delta + (F_{xfl} + F_{xfr}) \sin \delta + F_{yrl} + F_{yrr}$$

$$(36) \quad J_z \ddot{\psi} = l_f (F_{yfl} + F_{yfr}) \cos \delta + l_f (F_{xfl} + F_{xfr}) \sin \delta - l_r (F_{yrl} + F_{yrr}) - \frac{d_f}{2} (F_{yfr} - F_{yfl}) \sin \delta + \frac{d_f}{2} (F_{xfr} - F_{xfl}) \cos \delta + \frac{d_r}{2} (F_{xrr} - F_{xrl})$$

$$(37) \quad \beta = \tan^{-1}(v_y/v_x)$$

$$(38) \quad F_a = \frac{1}{2} \rho C_d A v_x^2$$

$$(39) \quad F_g = m_v g \sin \theta_r$$

$$(40) \quad F_r = m_v g C_r$$

Where: m_v – vehicle mass; a_x , a_y – lateral and longitudinal accelerations respectively; δ – road steering angle of front wheel; β – the vehicle body slip angle; l_f , l_r – distances from front and rear axle respectively to centre of gravity; d_f , d_r – front and rear track widths respectively; v_x – longitudinal velocity; v_y – lateral velocity; ψ – yaw rate; J_z – the yaw moment of inertia; F_{xij} – tire longitudinal forces, F_{yij} – tire lateral forces, (i represents the front and rear axles, j represents the left and right wheel); F_a – the aerodynamic drag force; F_g – The downgrade force; F_r – the rolling resistance force; ρ – the air density; A – the vehicle cross sectional area; C_r – the rolling resistance coefficient; θ_r – the road angle.

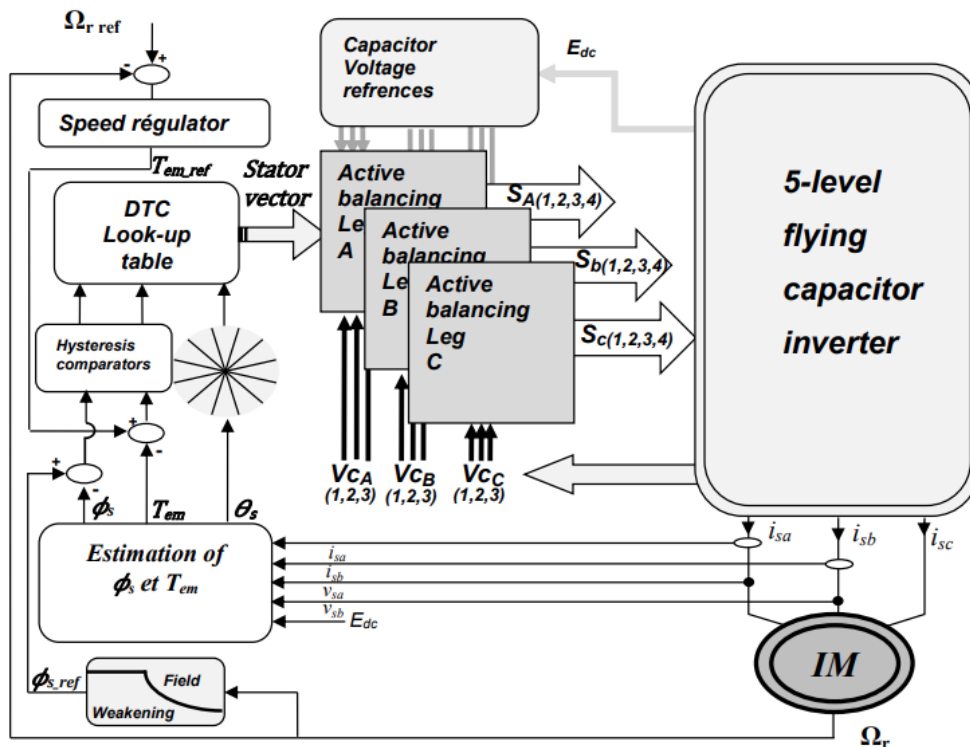


Fig. 5. Proposed structure of DTC scheme for induction machine fed by 5 level flying capacitor inverter with active balancing

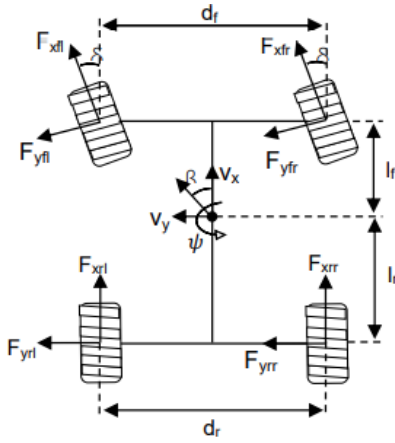


Fig. 6. The 7-DOF vehicle model

The rotational dynamics of the four tires are given by :

$$(41) \quad J_w \dot{\omega}_{fl} = T_{dfl} - T_{bfl} - F_{xfl} R_e$$

$$(42) \quad J_w \dot{\omega}_{fr} = T_{dfr} - T_{bfr} - F_{xfr} R_e$$

$$(43) \quad J_{tot3} \dot{\omega}_{rl} = T_{drl} - T_{brl} - F_{xrl} R_e$$

$$(44) \quad J_{tot4} \dot{\omega}_{rr} = T_{drr} - T_{brr} - F_{xrr} R_e$$

Where: $T_{dij}, T_{bij}, \omega_{ij}$ – Driving torque, braking torque and rotational velocity of wheel (ij) respectively; R_e – the effective radius of the tire.

Since there is an open differential for RWD (Fig. 7), the effective inertia J_{tot3}, J_{tot4} at rear left wheel and rear right wheel levels are given respectively as [18]:

$$(45) \quad J_{tot3} = J_w + J_l + (J_{cage}/2) + ((J_m + J_{input})N_D^2)/2$$

$$(46) \quad J_{tot4} = J_w + J_r + (J_{cage}/2) + ((J_m + J_{input})N_D^2)/2$$

The open differential delivers equal amount of torque to Left rear wheel and right rear wheel (assuming an infinitely high torsional stiffness for left and right shafts. It is also assumed that the efficiency of the open differential is 100%), thus, we can write :

$$(47) \quad T_{drl} = T_{drr} = 0.5 N_D T_{em}$$

Where: N_D – the main gear reduction ratio.

The relation between the rotational speeds of the left and right wheels and motor speed can be given as:

$$(48) \quad \Omega_r = \frac{N_D}{2} (\omega_{rl} + \omega_{rr})$$

The normal loads experienced by each tyre according to the weight transfer due to lateral and longitudinal accelerations (a_x and a_y) [19], can be written as:

$$(49) \quad F_{zfl} = m_v \left(\frac{l_r}{l_f + l_r} g - \frac{h}{l_f + l_r} a_x \right) \left(\frac{1}{2} - \frac{h a_y}{d_f g} \right)$$

$$(50) \quad F_{zfr} = m_v \left(\frac{l_r}{l_f + l_r} g - \frac{h}{l_f + l_r} a_x \right) \left(\frac{1}{2} + \frac{h a_y}{d_f g} \right)$$

$$(51) \quad F_{zrl} = m_v \left(\frac{l_f}{l_f + l_r} g + \frac{h}{l_f + l_r} a_x \right) \left(\frac{1}{2} - \frac{h a_y}{d_r g} \right)$$

$$(52) \quad F_{zrr} = m_v \left(\frac{l_f}{l_f + l_r} g + \frac{h}{l_f + l_r} a_x \right) \left(\frac{1}{2} + \frac{h a_y}{d_r g} \right)$$

Where: h – the height of vehicle center of gravity The tire longitudinal slip ratio (k) are defined as:

$$(53) \quad k_{ij} = \frac{R_e \omega_{ij} - \dot{x}_{w,ij}}{\max(R_e \omega_{ij}; \dot{x}_{w,ij})}$$

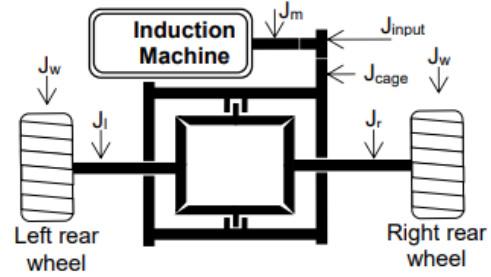


Fig. 7. Electric vehicle drivetrain architecture (RWD) and associated inertias

The longitudinal velocity of each wheel hub is required for the above longitudinal slip ratio (k) calculation, and can be derived [17] :

$$(54) \quad \dot{x}_{w,fl} = \left(v_x - \frac{\psi d_f}{2} \right) \cos \delta + (v_y + \dot{\psi} l_f) \sin \delta$$

$$(55) \quad \dot{x}_{w,fr} = \left(v_x + \frac{\psi d_f}{2} \right) \cos \delta + (v_y + \dot{\psi} l_f) \sin \delta$$

$$(56) \quad \dot{x}_{w,rl} = \left(v_x - \frac{\psi d_r}{2} \right)$$

$$(57) \quad \dot{x}_{w,rr} = \left(v_x + \frac{\psi d_r}{2} \right)$$

The slip angle of each wheel can be given as:

$$(58) \quad \alpha_{fl} = \delta - \tan^{-1} \left(\frac{v_y + l_f \dot{\psi}}{v_x - d_f \dot{\psi} / 2} \right)$$

$$(59) \quad \alpha_{fr} = \delta - \tan^{-1} \left(\frac{v_y + l_f \dot{\psi}}{v_x + d_f \dot{\psi} / 2} \right)$$

$$(60) \quad \alpha_{rl} = -\tan^{-1} \left(\frac{v_y - l_r \dot{\psi}}{v_x - d_r \dot{\psi} / 2} \right)$$

$$(61) \quad \alpha_{rr} = -\tan^{-1} \left(\frac{v_y - l_r \dot{\psi}}{v_x + d_r \dot{\psi} / 2} \right)$$

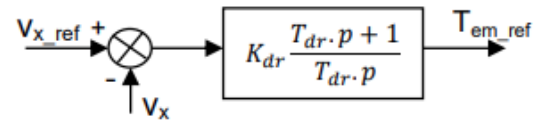


Fig. 8. Driver model

Combined slip Tire model

A combined slip tire model take into account the effects of simultaneous change of longitudinal tire slip ratio and tire slip angle on the longitudinal and lateral forces, first, the longitudinal tire force with pure Longitudinal Slip ($\alpha=0$), and lateral tire force with pure side angle ($k=0$) are calculated using magic formula tire model [20]:

$$(61) \quad F_{x0} = D_x \sin(C_x \tan^{-1}(B_x k_x - E_x(k_x - \tan^{-1}(B_x k_x)))) + S_{vx}$$

$$(62) \quad k_x = k + S_{hx}$$

$$(63) \quad F_{y0} = D_y \sin(C_y \tan^{-1}(B_y \alpha_y - E_y(\alpha_y - \tan^{-1}(B_y \alpha_y)))) + S_{vy}$$

$$(64) \quad \alpha_y = \alpha + S_{hy}$$

The magic formula coefficients $B_x, C_x, D_x, E_x, S_{vx}$ and S_{hx} for pure Longitudinal force and the coefficients $B_y, C_y, D_y, E_y, S_{vy}$ and S_{hy} for pure laterale force are caculed as deccribed in Appendix (see Table. 5 and 6).

The magic formula parameters b_0 through b_{12} and a_0 through a_{13} are often determined from the measurement data. In this work, we use the parameters presented in [20]. To combine longitudinal and lateral forces, Beckman has proposed a simple method based on friction circle [21]. First, it is necessary to find the values of longitudinal slip (k) for which $f_{x0}(F_z, k)$ has its maximum, and the values of side slip angle (α) for which $F_{y0}(F_z, \alpha)$ has its maximum, call these two values $\bar{k}, \bar{\alpha}$. To scaling k et α , we define new non dimensional quantities s and a as follows :

$$(65) \quad s = k/\bar{k}$$

$$(66) \quad a = \alpha/\bar{\alpha}$$

We can write new functions $\Phi_x(s) = F_{x0}(k)$ and $\Phi_y(a) = F_{y0}(\alpha)$ which have their maxima at $s=1$ and $a=1$. According to the criteria of Beckman, The combined slip model for tire will be set as follows:

$$(67) \quad F_x(s, a) = \frac{s}{\tau} \Phi_x(\tau), \quad F_y(s, a) = \frac{a}{\tau} \Phi_y(\tau), \quad \tau = \sqrt{s^2 + a^2}$$

Driver model

The driver behavior (see Fig. 8) used in this work takes account only the longitudinal dimension, it is simulated by PI controller where integral time constant T_{dr} corresponds to the driver reaction time [22]:

$$(68) \quad T_{dr} = 4T_T$$

$$(69) \quad K_{dr} = \frac{R_e m_v}{2T_T K_T}$$

The hand wheel angle (θ_h) will be considered as an input independently of longitudinal driver model, we assume a linear relation between θ_h and the road steering angle (δ) given as:

$$(70) \quad \theta_h = S_r \delta$$

Where : S_r – The steering ratio.

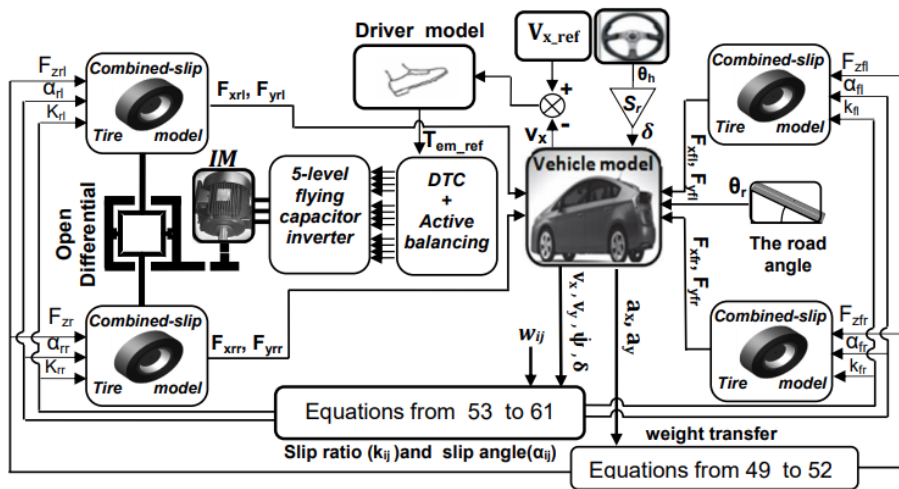


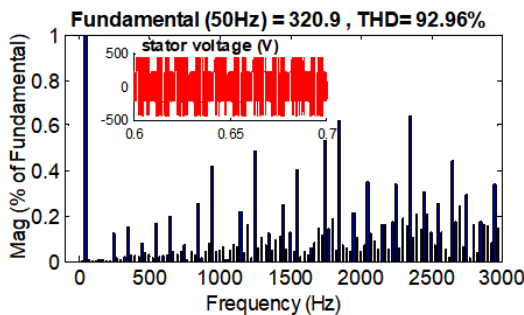
Fig. 9. Schematic diagram of electric vehicle with global control proposed

Simulation results

The proposed structure of control presented is extensively simulated in matlab/simulink, we propose dividing simulations into sections, first, we evaluate the effectiveness of structure of DTC-induction machine fed by 5 level flying capacitor inverter with active balancing (see Fig. 5), separately to the electric vehicle drivetrain, the results of this part will be presented from Fig. 10 to Fig. 16, the second section will be devoted to the global structure as presented in Fig. 9.

The characteristics of the induction machine and vehicle parameters used are given in appendix (see Table. 3 and 4).

a)



b)

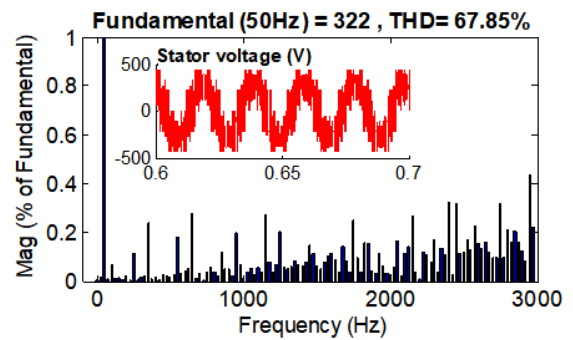
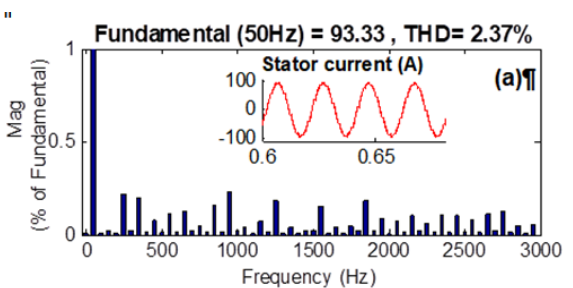


Fig.10. Stator voltage and its harmonics spectrum for : (a) DTC 2-level inverter. (b) DTC 5-level inverter.



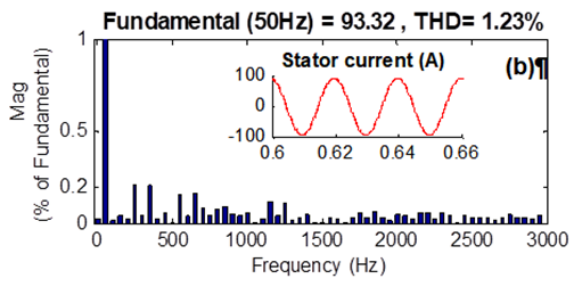


Fig. 11. Stator current and its harmonics spectrum for: (a) DTC 2-level inverter. (b) DTC 5-level inverter

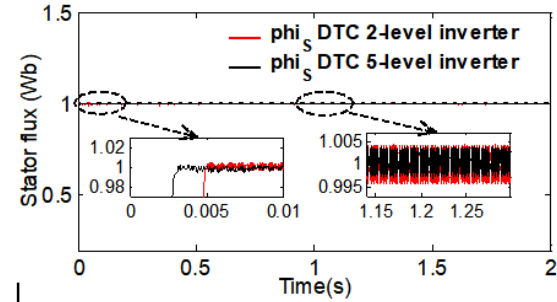


Fig. 12. Stator flux magnitude

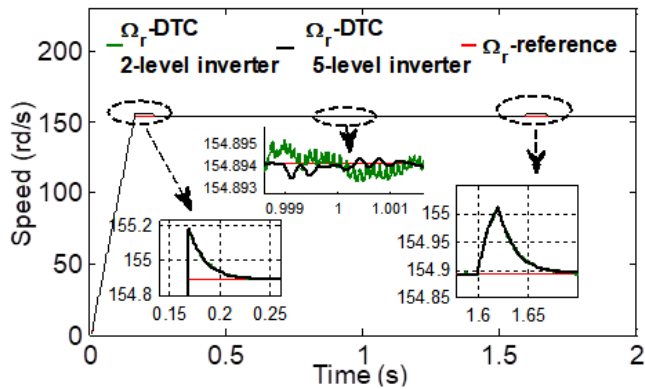


Fig. 13. Rotor speed

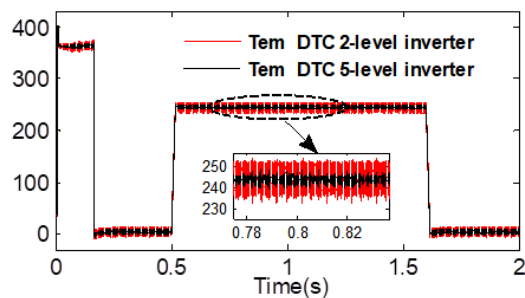


Fig. 14. Electromagnetic torque

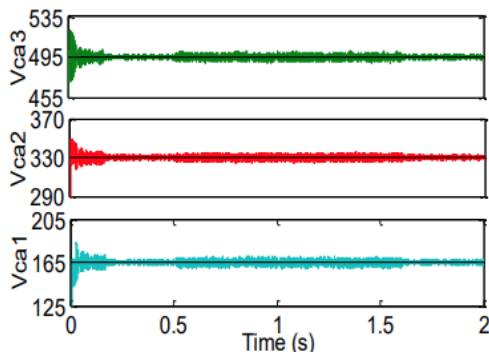


Fig. 15. Leg-A capacitor voltages

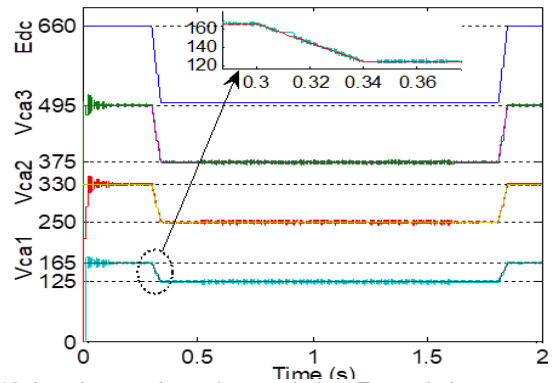


Fig. 16. Leg-A capacitor voltages during E_{dc} variation

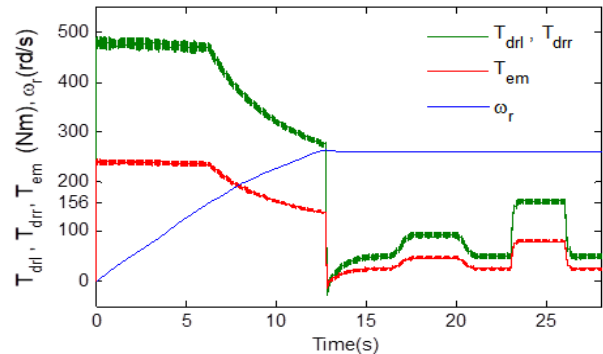


Fig. 17. Driving torque applied to wheels, motor torque, motor speed

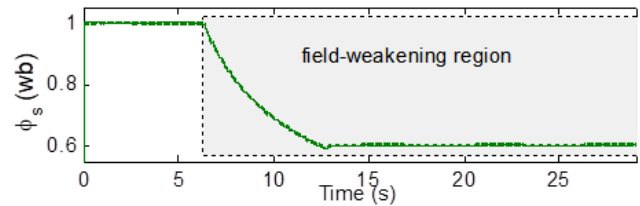


Fig. 18. Stator flux magnitude

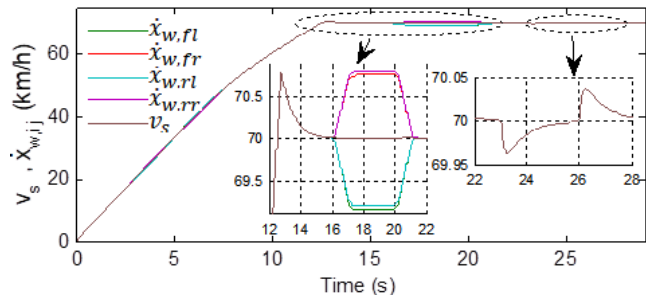


Fig. 19. Linear wheel velocities, Longitudinal velocity

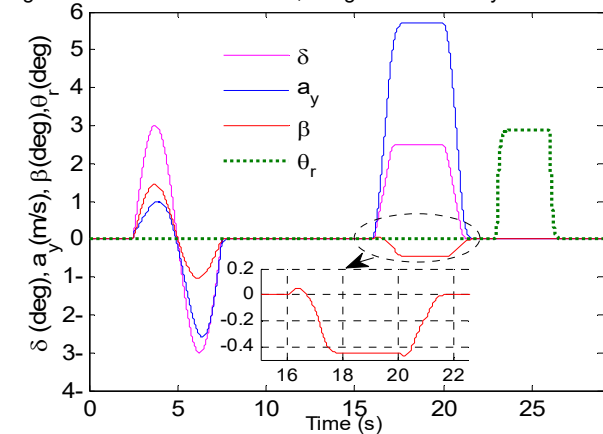


Fig. 20. Road steering angle, lateral acceleration, vehicle body slip angle, road angle

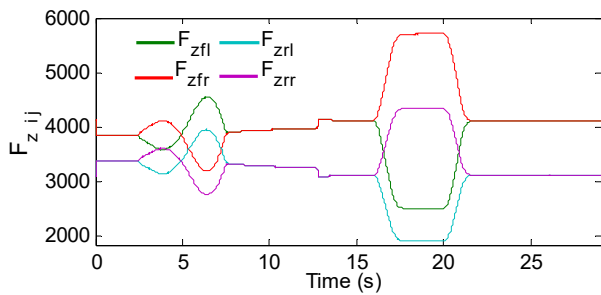


Fig. 21. Normal load by each tire

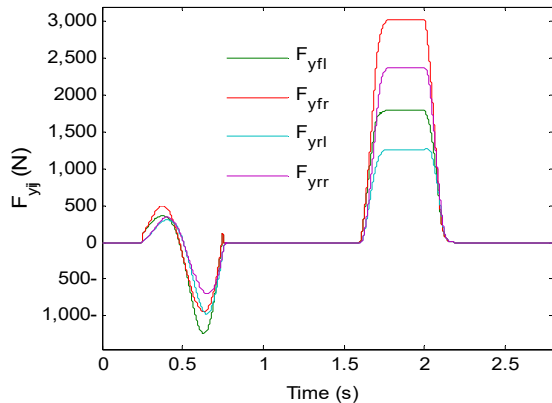


Fig. 22. Tire lateral forces

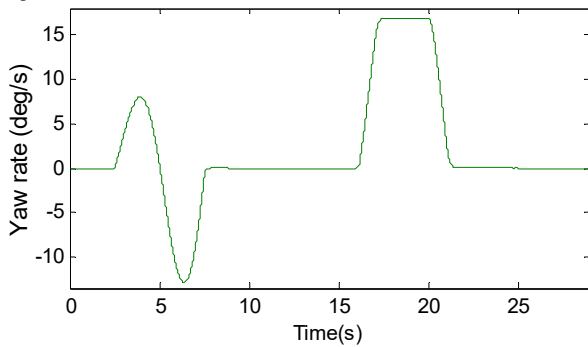


Fig. 23. Yaw rate

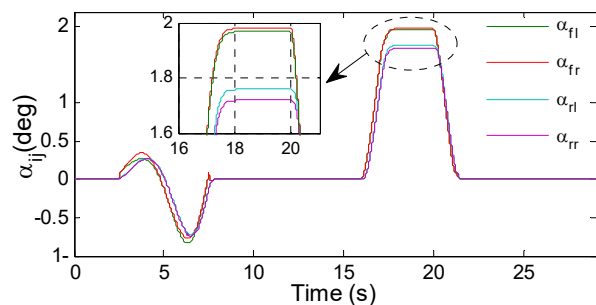


Fig. 24. Tire slip angles

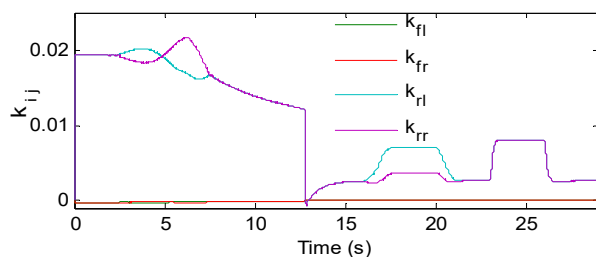


Fig. 25. Tire Longitudinal slip ratio

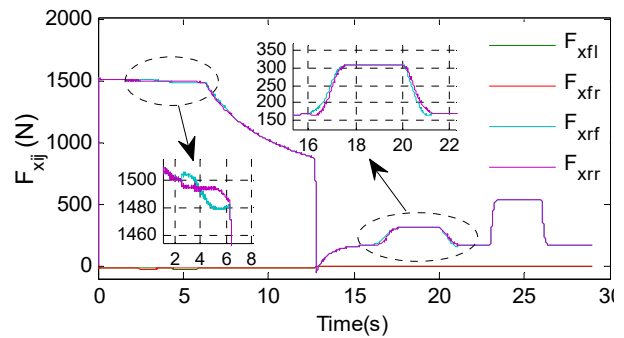


Fig. 26. Tire longitudinal forces

Analysis & discussion - First section

In order to present a detailed comparison between DTC-2-level inverter and DTC 5-level flying capacitor inverter, the simulation test have been carried under similar operating conditions and with the same type of speed regulator, namely, Proportional Intergrator (PI) regulator. The test is organized as follows, the machine starts without load with a raising ramp for speed reference from $t=0s$ to $t=1.17s$ to achieve 154.9 rd/s. At $t=0.5$, a 100% load torque (T_m) was applied, and at $t=1.6s$, the load torque was removed, the test ends at $t=2s$.

The voltage curves and their harmonics spectrum are shown in Fig.10, It can clearly be seen the reduction of THD from 92.96% for DTC 2-level to 67.85 for DTC 5-level inverter, the same case for stator current (see Fig. 12), the THD decrease from 2.37 to 1.23, this improvement of the voltage and current quality provided in DTC 5-level inverter, It was also manifested by low ripple in both electromagnetic torque and stator flux as shown in Fig.12 and Fig.14.

In Fig.13 the rotor speed reach its reference very fast and disturbance rejection due to load torque is rapid in both DTC 2-level and DTC 5-level.

As already stated, the independence active balancing Between three legs of 5-level flying capacitors gives us the choice to present only one leg, the same strategy of balancing are used in the other legs.

The Fig. 15 shows clearly very satisfactory performance for active balancing control ,a good tracking with fast reponse by the capacitor voltages of leg-A with voltage references.

To verify in further detail the robustness and efficiency of the active balancing for 5 level flying capacitor inverter, we present a second simulation test, a falling ramp variation of 160 V of E_{dc} occurs at $t = 0.3 s$ and ends at $t = 0.34 s$. At $t=1.81s$, a raising ramp variation restores the initial value of E_{dc} . The load torque was applied between $t=0.5s$ and $t=1.62s$, the reference speed is 100 rd/s, the test ends at $t=2s$, the results of this test are presented in Fig. 16.

The active balancing proposed shows a very good robustness against change in E_{dc} with a remarkable pursuit between capacitor voltages and their references without affecting the DTC control and proposed speed regulation.

Analysis & discussion - Second section

In order to verify the performance of proposed control of electric vehicle, we propose the following driving conditions:

- The road friction coefficient μ is assumed to be one.
- The reference speed is 70 km/h.
- Two steering senarios, first is sine wave from $t=2.5s$ to $t=7.5 s$, its peak value is $\theta_h=45 \text{ deg}$ ($\delta =3 \text{ deg}$). Second, a raising ramp variation of 37 deg of θ_h ($\delta = 2.5 \text{ deg}$) occurs

at $t=16$ s and ends at $t=17$ s. At $t=20$ s, a falling ramp variation restores the zero value of θ_h .

Fig. 17 shows the electromagnetic torque developed by Induction motor and the driving torques applied to rear wheels. Under different operating regions of induction motor (constant torque region and constant power region), the open differential ensure its function for increasing the drive torque and providing the same torque to left and right wheels.

In constant power region, as the speed increase, the stator flux reference decrease automatically according to field weakening algorithm as shown in Fig. 18.

The final motor speed is about 170% of the based speed, The filed weakening strategy shows a stability to enable this high speed for EV Operating conditions.

The longitudinal velocity (v_s) track the reference speed in 12 s. During the turn, the linear velocities of outer wheels are bigger than those of the inner ones to ensure VE stability during cornering as shown Fig. 20.

It can be observed in Fig 20, 22, 23, 24, that, yaw rate, lateral acceleration, vehicle body slip angle and tire lateral forces are manifested only during the turn, and they vanish on a straight road, their form are identical to road steering angle but their amplitudes are different.

In fact, it should be noted that, as the EV stability criterion, yaw rate and vehicle body slip angle, they must not exceed the limits given by [23] :

$\dot{\psi}_{upper} = (085 * \mu * g / v_s)$, $\beta_{upper} = \tan^{-1}(0.02\mu g)$, which are verified in the control proposed.

The Fig. 25 shows longitudinal slip ratio of tires, it can be observed that their values maintained lower than 2% for driving wheels, and for front wheels, their values are Very small comparatively to rear wheels due to the lack of driving torque.

The longitudinal forces of rear wheels presented in Fig. 26 show the same waveform of driving torques in Fig. 18, because the latter are directly dependent on longitudinal forces.

The weight transfer due to lateral and longitudinal accelerations is clearly visible in the normal load acting on each tire as shown in Fig. 21.

Conclusion

In this paper, we have presented the direct torque control of 5-level flying capacitor inverter for induction machine drive dedicated to the electric vehicle control. The main objective of this study consists in improving and enhancing the electric propulsion system.

As it has been shown in the simulation results, the insertion of 5 level inverter ensures a better performances in the stator voltage and current quality manifested also by low ripple in both electromagnetic torque and stator flux.

It has been verified that, the capacitor voltages have successfully balanced basing only on configuration selection by each leg, this active balancing provides a best robustness during E_{dc} variation.

The electric vehicle powertrain architecture using single induction motor and open differential controlled by 5-level inverter with DTC control gives a satisfactory performance with stability of electric vehicle under several driving conditions presented in this work.

Appendix

Table 3. Induction machine parameters

	Stator voltage-frequency	230/400 V-50 Hz
P_n	Rated power	37 Kw
Ω_b	Rated speed	155 rd/s
R_s	Stator resistance	0.08233 Ω

R_r	Rotor resistance	0.0503 Ω
L_s	Stator inductance	0.0278 H
L_r	Rotor inductance	0.0278 H
M	Mutual inductance	0.02711 H
P	Number of pole pairs	2
J_m	Motor inertia	0.37 $Kg.m^2$
f_r	Friction coefficient	0.02791 $Nm.s/rad$
E_{dc}	DC voltage	660 V
C	Inverter capacitances	200 μF

Table 4. Vehicle parameters

Symbol	Value	Symbol	Value
m_v	1476 (Kg)	S_r	15
l_f	1.127 (m)	K_T	1
l_r	1.485 (m)	T_T	0.2
d_f	1.5 (m)	N_d	4
d_r	1.5 (m)	R_e	0.3 (m)
h	0,5 (m)	J_z	2100 (Kgm^2)
A	1.8 (m^2)	J_w	1 (Kgm^2)
g	9.81 (m/s^2)	J_l	0.01 (Kgm^2)
ρ	1.224 (Kg/m^3)	J_r	0.01 (Kgm^2)
C_d	0.3 (m)	J_{cage}	0.1 (Kgm^2)
C_r	0.015	J_{INPUT}	0.02 (Kgm^2)

Table 5. The magic formula coefficients for F_{x0}

the meaning of the coefficient	formula
The Peak value	$D_x = b_1 F_z^2 + b_2 F_z$
The Shape Factor	$C_x = b_0$
Cornering stiffness	$B_x C_x D_x = (b_3 F_z^2 + b_4 F_z) \exp(-b_5 F_z)$
Stiffness factor	$B_x = (B_x C_x D_x / C_x D_x)$
The curvature factor	$E_x = b_6 F_z^2 + b_7 F_z + b_8$
The horizontal shift	$S_{hx} = b_9 F_z + b_{10}$
The vertical shift	$S_{vx} = b_{11} F_z + b_{12}$

Table 6. The magic formula coefficients for F_{y0} ($\gamma = 0$)

the meaning of the coefficient	formula
The Peak value	$D_y = a_1 F_z^2 + a_2 F_z$
The Shape Factor	$C_y = a_0$
Cornering stiffness	$B_y C_y D_y = a_3 \sin(2 \tan^{-1}(F_z/a_4))(1 - a_5 \gamma)$
Stiffness factor	$B_y = (B_y C_y D_y / C_y D_y)$
The curvature factor	$E_y = \min(a_6 F_z + a_7; 1)$
The horizontal shift	$S_{hy} = a_8 \gamma + a_9 F_z + a_{10}$
The vertical shift	$S_{vy} = (a_{111} + a_{112} F_z) \gamma F_z + a_{12} F_z + a_{13}$

Authors. Abderrahmen GUEBLI, Mohamed ABID, Abdelghani AISSAOUI, Abdellatif NACERI, IRECOM Laboratory, Department of Electrical Engineering, Faculty of Electrical Engineering, Djillali Liabes University, Sidi Bel-Abbes, Algeria
Email : aguebli@outlook.com.

REFERENCES

- [1] Lokriti A., Zidani Y., Doubabi S., Fuzzy logic control contribution to the direct torque and flux control of an induction machine, *IEEE International Conference on Ouarzazate*, 7-9 April 2011.
- [2] Ouboubker L., Khafallah M., Lamterkati J., Chikh K., Comparison between DTC using a two-level inverters and DTC using a three level inverters of Induction Motor, *2014 International Conference on Multimedia Computing and Systems*, Marrakech, Morocco, 2014.

- [3] Priya S., Suresh A., Rashmi M. R., GCMT-249 Investigation and Performance Analysis of Direct Torque Control of 3phase Induction Motor using 7 Level Neutral Point Clamped Multilevel Inverter, *Indian J. Sci. Technol.*, vol. 9, pp. 1-7, 2016.
- [4] Bouarfa A., Bodson M., Fadel M., A fast active-balancing method for the 3-phase multilevel ying capacitor inverter derived from control allocation theory, *International Federation of Automatic Control*, Papers On Line 50-1, (2017), 2113–2118.
- [5] Norambuena, M., Lezana, P., Rodriguez, J., A simple modulation strategy for a Flying Capacitor Converter using Predictive Control, *IEEE IECON*, Florence, Italy.2016.
- [6] Tachon, O., Fadel M., Meynard T., Control of series multicell converters by linear state feedback decoupling., European conference on power electronics and applications, Trondheim, Norway, vol. 1. p.588-1.593, 1997.
- [7] Martins C A., Controle directe du couple d'une machine asynchrone alimentée par un convertisseur multiniveau a frequence imposée, thèse de doctorat, *Institut national polytechnique*, Toulouse, France, 2000.
- [8] Nordin N. M., Idris N. R. N., N. a. Azli, Direct torque Control with 5-level cascaded H-bridge multilevel inverter for induction machines, *IECON 2011 - 37th Annu. Conf. IEEE Ind. Electron. Soc*, pp. 4691-4697, 2011.
- [9] Tarusan S. A. A., Jidin A., Jamil M. L. M., Abdul Karim K, Sutikno T., A review of direct torque control development in various multilevel inverter applications, *International Journal of Power Electronics and Drive System*, Vol. 11, No. 3, September 2020, pp. 1675~1688.
- [10] Chandrasekhar O., five-level svm inverter for an induction motor with direct torque controller, *Journal of Electrical Engineering*, December 2013.
- [11] Casadei D., Serra G., Stefani A., Tani A., and Zarri L., DTC Drives for Wide Speed Range Applications Using a Robust Flux-Weakening Algorithm, *IEEE Transactions on Industrial Electronics*, VOL. 54, NO. 5, OCTOBER 2007.
- [12] Tarchala G., Orłowska-Kowalska T., Nguyen Thac K, Dybkowski M., Performance analysis of the sensorless direct torque controlled induction motor drive with optimal field weakening algorithm in traction applications, *Przegląd Elektrotechniczny*, 88(11):12-16, January 2012.
- [13] Kumar Singh A., Reddy U., Kumar Prabhakar K., Kumar P., Selection of Reference Flux Linkage for Direct Torque Control Based Induction Motor Drive in Electric Vehicle Applications, *SAE International. J. Alt. Power. / Volume 8, Issue 1*, 2019.
- [14] De Klerk M L., Saha A K., Performance analysis of DTC-SVM in a complete traction motor control mechanism for a battery electric vehicle, *Heliyon 8*, (2022) e09265.
- [15] Nguyen Thac K., Tarchala G., Orłowska-Kowalska T., Comparative analysis of the chosen field-weakening methods for the Direct Rotor Flux Oriented Control drive system, *Archives of electrical Engineering*, VOL. 61(4), pp. 443-454 (2012).
- [16] Genta G., Motor vehicle dynamics: modeling and simulation, *Series on Advances in Mathematics for Applied Sciences. World Scientific Publishing Co. Pte.Ltd*, Vol. 43, 1997.
- [17] Parker G., Griffin J., Popov A., The effect on power consumption & handling of efficiency-driven active torque distribution in a four wheeled vehicle, *The Dynamics of Vehicles on Roads and Tracks, proceeding IAVSD 2015*, Graz, Austria, 17–21 August 2015.
- [18] Bayar K., Performance comparison of electric-vehicle drivetrain architectures from a vehicle dynamics perspective, *J Automobile Engineering*, 1–21, IMechE 2019.
- [19] Jalali K., Uchida T., Lambert S., McPhee, J., Development of an Advanced Torque Vectoring Control System for an Electric Vehicle with In-Wheel Motors using Soft Computing Techniques, *SAE International*, 2013-01-0698.
- [20] Niesner C., Sensibilité et robustesse à l'incertitude paramétrique: une approche Bond Graph, Thèse de doctorat, *Université des sciences et technologies de Lille*, 2005.
- [21] Beckman B., Physics of Racing, Part 25 : Combination grip, 1992, p. 116–121.
- [22] Cipek M., Pavkovic D., Joško P., A control-oriented simulation model of a power-split hybrid electric vehicle, *Applied Energy*, 2012.
- [23] Lia L., Jiaa G., Chena J., Zhua H., Caob D., J Song, A novel vehicle dynamics stability control algorithm based on the hierarchical strategy with constrain of nonlinear tyre forces, *Vehicle System Dynamics, International Journal of Vehicle Mechanics and Mobility*, 2015.